Available online at www.sciencedirect.com
ScienceDirect
Journal of Power Sources 160 (2006) 775–781
JOURNAL OF POWER SOURCES
www.elsevier.com/locate/jpowsour

Porous nickel MCFC cathode coated by potentiostatically deposited cobalt oxide
II. Structural and morphological behavior in molten carbonate

M.J. Escudero [a,*], L. Mendoza [b], M. Cassir [b], T. Gonzalez [a], L. Daza [a,c]

[a] *Dpto. Energía, CIEMAT, Av. Complutense 22, 28040 Madrid, Spain*
[b] *Instituto de Catálisis y Petroleoquímica (CSIC), Campus Cantoblanco, 28049 Madrid, Spain*
[c] *Ecole Nationale Supérieure de Chimie de Paris, Laboratoire d'Electrochimie et de Chimie Analytique (UMR 7575 CNRS), 11 rue Pierre et Marie Curie, 75231 Paris Cedex 05, France*

Available online 30 May 2006

Abstract

Cobalt oxide was deposited on porous nickel by an electrodeposition technique as precursor of a novel MCFC cathode. The behavior of this cathode in molten $(Li_{0.52}Na_{0.48})_2CO_3$ eutectics at 650 °C under an atmosphere of CO_2:air (30:70) was studied before and after 50 h of exposure by different techniques. Before the exposure, the deposit of cobalt corresponded to a Co_3O_4 thin layer of. This crystalline structure was identified by XRD and Raman spectroscopy. After its exposure in the eutectic melt a loss of cobalt was observed by XRD, Raman spectroscopy, XPS, EDS and ICP-AES. The change in the Co_3O_4 structure into lithium–cobalt–nickel oxide ($LiCo_{1-y}Ni_yO_2$) was observed by Raman spectroscopy. The SEM micrographs for Co_3O_4-coated porous nickel showed different angular shapes with respect to porous Ni. The nickel solubility for the coated porous nickel, measured by ICP-AES, decreased with respect to uncoated nickel. The Co_3O_4-coated porous nickel cathode showed, after its immersion in the molten carbonate melt, a similar porosity but a higher pore size. $LiCo_{1-y}Ni_yO_2$-coated NiO offers interesting features which combine the properties of nickel, lithium and cobalt in molten carbonate. This could be a promising novel MCFC cathode material.

Keywords: EIS; Raman; Cobalt oxide; Cathode; Molten carbonate fuel cell

1. Introduction

The large-scale commercialization of molten carbonate fuel cell (MCFC) is limited by its relatively short lifetime mainly due to the dissolution of the state-of-art nickel oxide cathode in molten carbonate and its structural degradation during the operation of the cell. Recently, the approach of developing alternative cathode materials has been directed to cover the pore surface of NiO cathode with a layer of protective materials to reduce its dissolution. NiO cathodes coated with $LiCoO_2$, $LiCo_{1-y}Ni_yO_2$, $LiFeO_2$, $La_{0.8}Sr_{0.2}CoO_3$ or $MgFe_2O_4$ as well as impregnated with cerium, lanthanum and cobalt have been studied [1–12].

$LiCoO_2$ was once considered the most promising alternative cathode material due to its extremely low solubility. However, $LiCoO_2$ is less electronically conductive than NiO, and is limited for producing large electrodes because of its brittleness and higher manufacturing cost than NiO [2,13]. Stoichiometric lithium nickel mixed oxides have a good electronic conductivity when is compared to other ceramic oxides like $LiCoO_2$ [14]; however, highly lithiated nickel oxides are not stable in the eutectic melt [15].

In this study, we propose a new porous nickel cathode coated with a layer of a cobalt oxide-based compound. The insertion of lithium into the NiO lattice increases the electronic conductivity [16], and the insertion of cobalt improves the stability of this new material in the carbonate melt [2]. The Li(Co, Ni) oxide coating is obtained by the in situ oxidation and lithiation of cobalt on porous nickel in the eutectic melt.

Various coating techniques, such as sol-impregnation [9], sol–gel [17], and electroplating [1] have been used to fabricate the precursors of $LiCo_{1-y}Ni_yO_2$-coated cathodes for MCFC. In all these techniques, the coating of Li(Co, Ni) oxide was obtained by in situ oxidation and lithiation in the eutectic melt of cobalt

* Corresponding author. Tel.: +34 913466622; fax: +34 913466269.
E-mail address: m.escudero@ciemat.es (M.J. Escudero).

0378-7753/$ – see front matter © 2006 Elsevier B.V. All rights reserved.
doi:10.1016/j.jpowsour.2006.04.056

deposits. The electrochemical deposition is a low cost technique and allows to control the coating thickness and morphology by varying different experimental parameters (concentration, fixed potential, potential steps, electrolysis duration, temperature and selection of the solvent and electrolyte) [11,12].

In the present work, cobalt oxide deposit was prepared on the porous nickel by potentiostatic deposition followed by a heat treatment as precursor of a novel MCFC cathode. The behavior of novel cathode in molten $(Li_{0.52}Na_{0.48})_2CO_3$ eutectics at 650 °C under a standard cathodic atmosphere of CO_2:air (30:70) was investigated. A pure porous nickel cathode was tested in the same conditions and taken as reference. The cathodes before and after its immersion in molten carbonate were analysed by different techniques.

2. Experimental

2.1. Electrochemical deposition

The sample was prepared by potentiostatic deposition of cobalt oxide film on porous nickel sample according to a procedure fully described in previous papers [11,12]. The deposition was performed in a four-compartment Tacussel glass cell with a 0.1 mol l^{-1} Co(II) solution prepared from $Co(NO_3)_2{\cdot}6H_2O$ in a 0.5 mol l^{-1} solution of $NaNO_3$ with a pH 4 under N_2 atmosphere at 25 °C. The pH was fixed at 7.4 by addition of a 1 mol l^{-1} NaOH solution. The working electrode was a porous nickel foil, the counter electrode was a Pt foil and the reference electrode was a $Hg|Hg_2Cl_2$ (SCE) which was placed in a separate compartment filled with a 0.5 mol l^{-1} $NaNO_3$. The potentiostatic deposition was performed with a Princenton applied research (PAR) model 263 system at 0.65 V versus SCE and an electrolysis times of 24 h. Then, the sample was annealing at 500 °C for 4 h in air at a heating rate of 1 °C min^{-1}.

2.2. Structural characterization and chemical analysis

The structure of cobalt oxide on porous nickel (NiO–Co) and porous nickel (NiO) was characterized before and after the electrochemical tests.

XRD analyses were performed with a Philips Model X'Pert-MPD diffractometter using a Cu Kα radiation (λ = 1.542 Å). The diffraction intensity was measured in the 2–90° (2θ) range, by steps of 0.05° (2θ) with a counting time of 2 s.

Raman spectra were obtained at room temperature with a Bruker RFS-100 FT-Raman spectrometer provided with a diode-pumped germanium solid-state detector, which operates at liquid N_2 temperature. A Nd:YAG laser was used as exciting source. The samples were pressed into the holder with no other pretreatment. A laser power of ca. 600 mW was used, the spectra being taken with a resolution 4 cm^{-1} and accumulating 500 scans. For each measurement the integration time was 30 min.

XPS analysis was performed with a Perkin-Elmer PHI 5400 spectrometer equipped with a Mg Kα excitation source ($h\nu$ = 1253.60 eV) and a beam size of 1 mm diameter. Typical operation conditions were: X-ray gun, 15 kV, 20 mA, pressure in the sample chamber ~10^{-9} Torr, pass energy, 89.50 eV for general spectra (0–1100 eV) and 35.75 eV for high resolution spectra. In order to take into account the charging effects on the measured binding energies, these energies were determined by referencing to the C 1s peak at 284.8 eV.

The morphology and the composition of the deposits were examined with SEM using a Hitachi microscope S-2500 combined with EDS, model Sun Sparcstation.

The content of nickel and cobalt in the eutectic melt was analysed by ICP-AES using a Jobin Yvon, JY-48/JY-38. The porosity and the pore size distribution were determined by mercury porosimetry using a Micrometrics Pore Sizer 9310.

3. Results and discussion

3.1. Structural characterization and chemical analysis

The structure of porous NiO–Co was studied by X-ray diffraction (XRD) before and after its exposure in the eutectic melt. As can be seen in Fig. 1, initially the XRD peaks correspond to metallic nickel at 44.50°, 51.84° and 76.37° (2θ), NiO at 37.28°, 42.23° and 62.97° (2θ) and Co_3O_4 at 19.00°, 31.27°, 59.35° and 65.23° (2θ). It was difficult to determine their crystalline structure due to the fact that cobalt oxides showed weaker intensity lines than those relative to nickel substrate. After its exposure during 50 h in the carbonate melt, we can observe the oxidation of nickel to NiO and the disappearance of the Co_3O_4 diffraction lines.

Raman spectra of porous NiO and porous NiO–Co before and after their exposure in molten carbonate are displayed in Fig. 2. The coated sample presents five bands at 197, 484, 523, 621 and 691 cm^{-1} that are not observed in the porous NiO. Co_3O_4 crystallizes in the normal spinel structure $Co^{2+}(Co^{3+})_2O_4{}^{2-}$ and belongs to the space group O_h^7-*Fd3m*. The spinel lattice is constituted by Co^{2+} and Co^{3+} placed at tetrahedral and octahedral sites, respectively. The active vibrations of spinel structure (*F3dm*) are

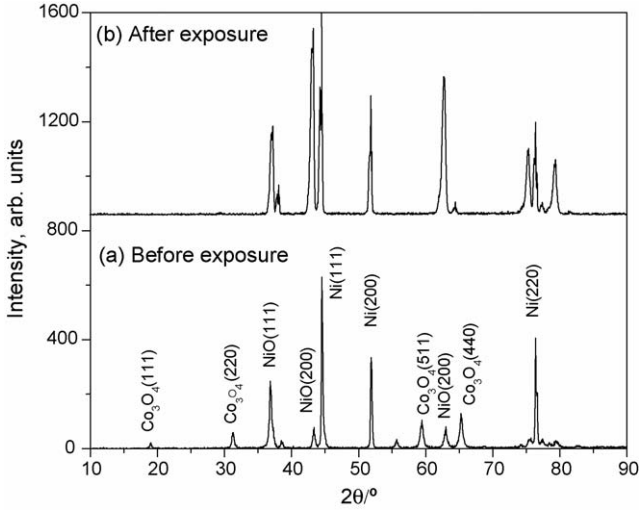

Fig. 1. XRD patterns obtained on a porous NiO–Co: (a) after heat treatment at 500 °C in air during 4 h; (b) after 50 h of exposure to $(Li_{0.52}Na_{0.48})_2CO_3$ at 650 °C under an atmosphere of CO_2:O_2:N_2 (30:15:55).

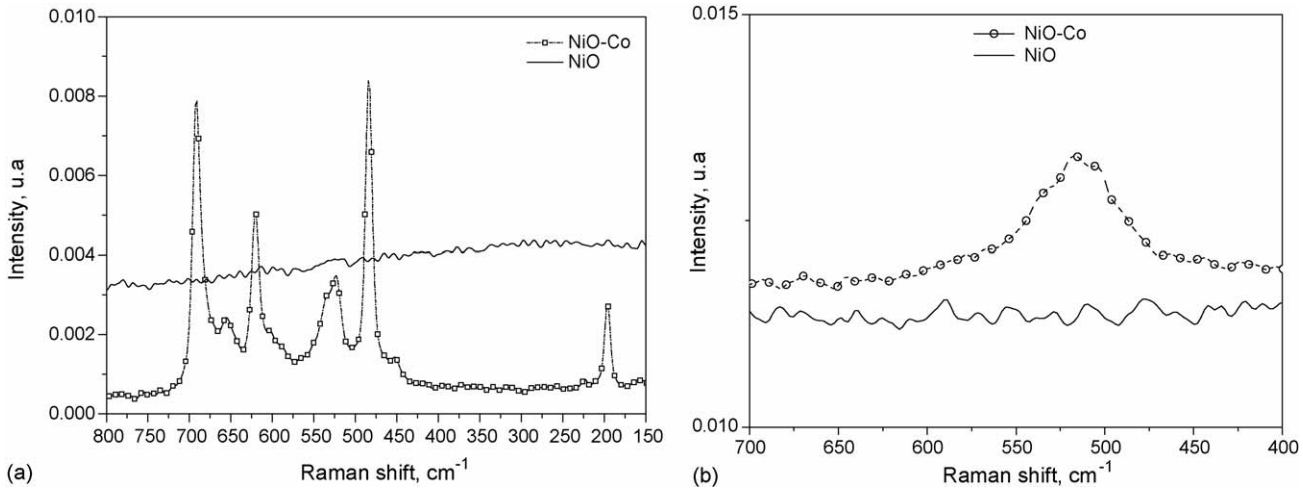

Fig. 2. Raman spectra of porous NiO and porous NiO–Co: (a) after heat treatment at 500 °C in air during 4 h; (b) after 50 h of exposure to $(Li_{0.52}Na_{0.48})_2CO_3$ at 650 °C under an atmosphere of CO_2:O_2:N_2 (30:15:55).

$A_{1g} + E_g + F_{1g} + 3F_{2g} + 2A_{2u} + 2E_u + 4F_{1u} + 2F_{2u}$. The A_{1g}, E_g and $3F_{2g}$ modes are Raman active, and $4F_{1u}$ are infrared active. The reaming F_{1g}, $2A_{2u}$, $2E_u$ and $2F_{2u}$ modes are inactive [18,19]. Therefore, the five Raman bands observed for the samples can be assigned to Raman active phones modes of Co_3O_4: the peaks at 197, 523, and 621 cm^{-1} correspond to F_{2g} phonon modes whereas the peaks at 484 and 691 cm^{-1} are E_g and A_{1g} phonon modes. The phonon symmetries determined in this work are in agreement with those given by Hadjiev et al. [18] and Herrera and Resasco [20]. Therefore, this confirmed that the crystalline structure of deposits corresponds to Co_3O_4 after the heat treatment.

After their exposure to carbonate melt at 650 °C during 50 h, the Raman spectrum of porous NiO–Co has only a broad band around 515 cm^{-1}, while the spectrum of porous NiO is almost featureless. The $LiCoO_2$ can be crystallized in a hexagonal structure with space group $R\bar{3}m$ or a spinel (cubic) structure with a space group $Fd3m$. The vibrations mode of crystalline $LiCoO_2$ in space groups $R\bar{3}m$ and $Fd3m$ were predicted by factor analysis groups [18,21,22]. The total vibrations modes of layered $LiCoO_2$ ($R\bar{3}m$) are $A_{1g} + E_g + 2A_{2u} + 2E_u$, where A_{1g} and E_g modes are Raman active, and $2A_{2u}$ and $2E_u$ modes are infrared active. Similarly, the total vibrations modes of spinel $LiCoO_2$ ($Fd3m$) are $A_{1g} + E_g + 2F_{2g} + 5F_{1u}$ where A_{1g}, E_g and $2F_{2g}$ are Raman active, and $5F_{1u}$ are infrared active. Inaba et al. [23] studied the Raman spectra of lithium–cobalt–nickel oxide, $LiCo_{1-y}Ni_yO_2$ ($0 \le y \le 1$) and observed two strong Raman band at 485 and 597 cm^{-1} for $LiCoO_2$ ($y = 0$). These peaks were assigned to A_{1g} and E_g vibrational modes in space group of $R\bar{3}m$. In the A_{1g} mode the two oxygen atoms vibrate in the opposite directions parallel to the c-axis of $LiCoO_2$, while they vibrate alternately in the opposite directions parallel to the Li and Co planes in the E_g modes. The intensities of both bands decreased drastically and the peak wavenumbers approached each other with increasing Ni content that replaces Co in $LiCo_{1-y}Ni_yO_2$. The Raman broad band observed in Fig. 2b for porous NiO–Co could be due to the formation of a lithium cobalt nickel oxide ($LiCo_{1-y}Ni_yO_2$) on the surface of nickel porous. The broad band at 515 cm^{-1} is in good agreement with the Raman peak reported 510 cm^{-1} by Kuk et al. [1] and Ryu et al. [24]. This difference could be probably due to the different electrolyte and gas composition, as well as the preparation method and composition of cobalt deposit.

The survey XPS spectra of NiO and NIO–Co before and after its exposure to eutectic melt at 650 °C under an atmosphere CO_2:air revealed the presence of O, Ni and C on the surface, as well as Co for the samples with deposits (also confirmed by the Auger lines). The binding energies (BEs) relative to Ni 2p, Co 2p and O 1s before and after their immersion in the carbonate melt sphere CO_2:air are presented in Table 1.

The position of skape-up satellites (ss) when appeared from the Ni 2p and Co 2p was also included, in order to aid identification of the chemical state. Curve fitting of O 1s signal, gives generally three contributions, the peaks O_I and O_{II} were assigned to oxide and hydroxide groups and/or non-stoichiometric surface oxygen, respectively. The third component, O_{III}, was attributed to molecular water adsorbed in the surface.

Initially, the Ni $2p_{3/2}$ and Ni $2p_{1/2}$ peaks for porous Ni presented a slightly lower of binding energies respect in comparison with the cobalt oxide on Ni porous. However, the signals shows poor resolution to identify appropriately the satellite bands associated to Ni (2p) spectrum. A deconvolution of Ni 2p revealed two main contributions for each Ni $2p_{3/2}$ and Ni $2p_{1/2}$ peak that were associated to NiO and $Ni(OH)_2$ due to the fact that the binding energies values are similar to the literature ones [25,26]. After exposure to the carbonate melt, the spectrum of porous Ni presents a $2p_{3/2}$ binding energy of 855.9 eV, a $2p_{1/2}$ binding energy of 873.5 eV, a strong shake up satellite 6.2 eV from the $2p_{3/2}$ peak and a strong shake up satellite at 5.9 eV from the $2p_{1/2}$ peak. Similar results were observed for the samples with cobalt oxide deposit. The XPS deconvolution of the Ni 2p peak revealed the contributions of Ni_2O_3, $Ni(OH)_2$ and NiO in both samples. The presence of Ni^{3+} could be associated to the lithiation process.

Table 1
XPS BEs of Ni 2p, Co 2p and O 1s peaks and shake-up satellites (ss) of Ni 2p for the porous NiO and the porous NiO–Co before and after 50 h of exposure to $(Li_{0.52}Na_{0.48})_2CO_3$ at 650 °C under an atmosphere CO_2:air (30:70)

	Before exposure		After exposure	
	NiO	NiO–Co	NiO	NiO–Co
Nickel				
Ni $2p_{3/2}$	855.5	855.9	856.0	855.9
ss	860.9	862.3	861.6	861.6
Ni $2p_{1/2}$	872.7	878.6	873.5	873.2
Cobalt				
Co $2p_{3/2}$		779.8		781.4
ss		789.4		
Co $2p_{1/2}$		794.7		796.0
Oxygen				
O $1s_I$	529.0 (O_I:32%)	529.6 (O_I:21%)	529.6 (O_I:37%)	529.4 (O_I:29%)
O $1s_{II}$	531.2 (O_{II}:53%)	531.2 (O_{II}:71%)	531.4 (O_{II}:47%)	531.1 (O_{II}:47%)
O $1s_{III}$	532.6 (O_{III}:15%)	533.3 (O_{III}:8%)	533.2 (O_{III}:16%)	532.9 (O_{III}:24%)

For cobalt, the spectra of cobalt oxide on porous nickel before and after its exposure are reported in Fig. 3. According to the literature, the Co $2p_{3/2}$ spectrum showed a complex structure broadened by multiplet splitting effects and in addition, very similar binding energies are known for most cobalt oxides and hydroxides (i.e. CoO, Co_2O_3, Co_3O_4, CoOOH) [11,25–27]. However, a detailed analysis of the Co 2p shake-up structure should allow the assignment to cobalt oxidation states.

In fact, it is well known that all the Co^{2+} compounds are high spin complexes with strong satellite bands, while all the Co^{3+} are diamagnetic [25,27]. At first, the Co $2p_{3/2}$ and Co $2p_{1/2}$ peaks at 779.8 and 794.7 eV and a weak satellite band appeared at 9.6 eV higher from the main peak and it is probably related to paramagnetic divalent high-spin cobalt. These results and the absence of strong shake-up satellite structure indicate the presence of Co_3O_4. Oxide-like CoO has intense satellite structures. These results are consistent with those reported by McIntyre and Cook [25] and Mitton et al. [26].

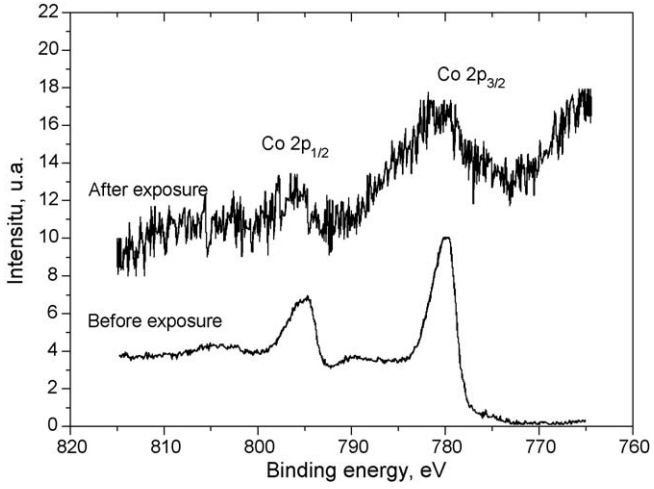

Fig. 3. Co 2p XPS spectra of NiO–Co: (a) after heat treatment at 500 °C in air during 4 h; (b) after 50 h of exposure to $(Li_{0.52}Na_{0.48})_2CO_3$ at 650 °C under an atmosphere of CO_2:O_2:N_2 (30:15:55).

As can be seen in Fig. 3, the Co 2p spectrum after the exposure in the molten carbonate confirmed the loss a cobalt and showed a poor resolution for the $2p_{3/2}$ peak at 781.4 eV and the $2p_{1/2}$ peak at 796.0 eV. Its deconvolution allowed to determine the contribution of $Co(OH)_2$ (57%) and Co_3O_4 and/or CoOOH (43%). The O 1s spectra exhibited a peak at low binding energies assigned to oxide species and a second peak at higher energies which correspond to hydroxide and carbonate ions. The concentrations of oxide, hydroxide and carbonate ions determined from the O 1s spectra for the Ni sample were 37%, 47% and 16%, respectively. For the cobalt oxide on nickel porous, the proportions of O 1s components were: 29% of oxide groups, 48% of OH^- groups and 24% of carbonate ions. The presence of carbonate groups in both samples was confirmed by the curve fitting to the C 1s region. Comparing both samples, similar concentration was determined in the hydroxide groups and the difference in the amount of carbonate and oxide groups could be related to an inappropriate removal of carbonate.

Therefore, XPS analysis of porous NiO and porous NiO–Co only confirmed the presence of Ni^{3+} that could be due to lithiation of both samples, but the formation of $LiCo_{1-y}Ni_yO_2$ layer could not be confirmed.

Fig. 4 represents the SEM micrographs for the porous NiO and the porous NiO–Co before and after their exposure. As shown in Fig. 5, the morphology of both samples are different due to the cobalt oxide deposition. The coated porous cathode in comparison with porous NiO presents more agglomeration and a granular structure.

Both samples suffered morphological changes after the exposure to the eutectic melt. For porous NiO, a slight morphological change, probably due to the lithiation process, can be observed. In the case of the coated porous sample a decrease in particle size can be observed, as well as different morphologies to porous NiO. This could be explained by the lithiated of Co/Ni

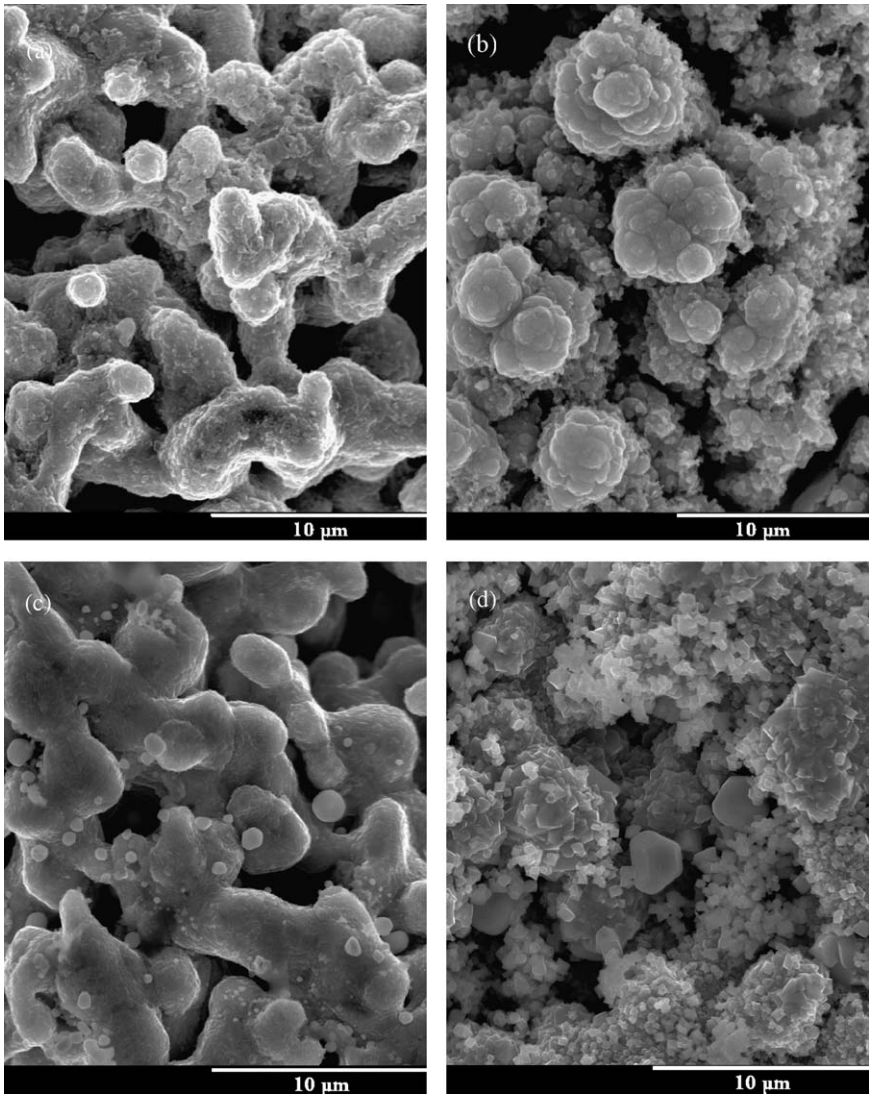

Fig. 4. SEM micrographs: (a) before exposure NiO; (b) before exposure NiO–Co; (c) after exposure NiO; (d) after exposure NiO–Co.

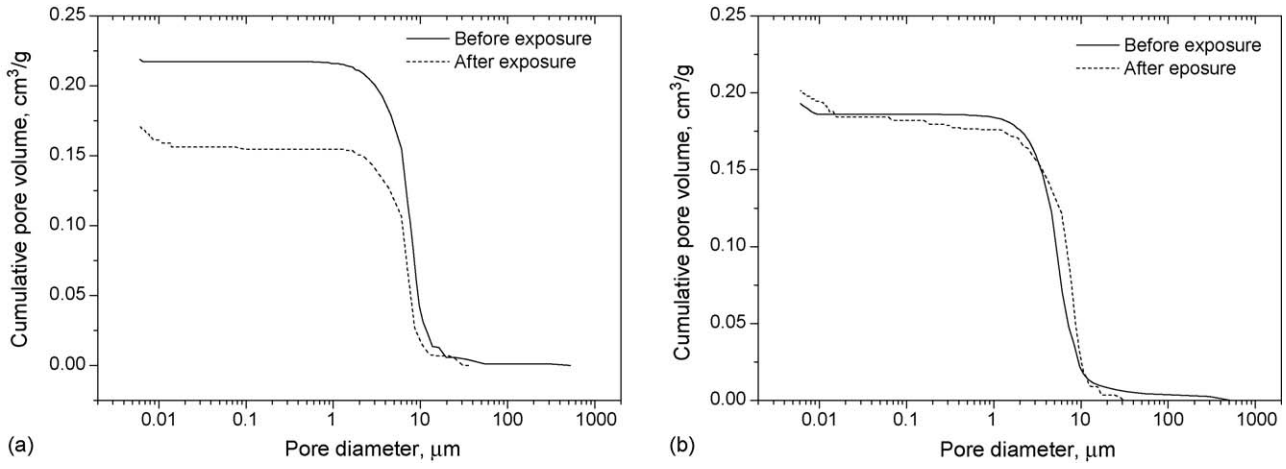

Fig. 5. Pore volume distribution before and after 50 h of exposure to $(Li_{0.52}Na_{0.48})_2CO_3$ at 650 °C under an atmosphere under an atmosphere of CO_2:O_2:N_2 (30:15:55). (a) Porous NiO; (b) porous Ni–Co.

in carbonate and the formation of a lithium cobalt nickel oxide ($LiCo_{1-y}Ni_yO_2$) on the surface of porous nickel. These results are in agreement with obtained by Raman studies.

EDS analyses confirmed the presence of cobalt after the immersion en molten carbonate melt during 50 h, but a 35% cobalt loss was detected.

Chemical analysis showed that both samples suffered a dissolution of nickel, but it was lower in the porous NiO–Co. The nickel content in the electrolyte was 11.0 wt.ppm in porous NiO. The electrolyte corresponds to porous NiO–Co presented a nickel content lower 5.5 wt.ppm, and a cobalt content 3.5 wt.ppm. This results confirmed the dissolution of cobalt, but an important reduction in the nickel solubility.

The cumulative pore volume and the porosimetric data for porous NiO and porous NiO–Co before and after theirs exposure to eutectic melt are given in Fig. 5a). Both samples exhibited an appropriate dual-pore structure with macro pores (>1 μm) and micro pores (<1 μm). This dual pore structure is a basic requirement for a MCFC cathode: the macro pores serve as gas channels for the fuel cell and the micro pores absorb molten electrolyte by capillary effects. Thus, the MCFC reduction reaction occurs in a ternary phase between the solid cathode phase, the molten electrolyte phase and the gas phase. After its immersion, the porous NiO sample shows, a lower pore distribution and pore diameter. This could be due to the lithiation process. The coated porous Ni presented similar pore distributions and porosity before and after its immersion. The pose size increased from 4.51 to 6.31 μm. This behavior may be due to a lithiation of Ni/Co on the surface. The coated porous sample presented a higher porosity and pore size than porous NiO. These properties could improve the cell performance.

4. Conclusions

Cobalt oxide was coated on the state-of-art MCFC nickel cathode by an electrodeposition technique. The behavior of on the deposits in molten carbonate at 650 °C during 50 h under CO_2:air (30:70) was investigated by XRD, Raman spectroscopy, XPS, SEM-EDS and mercury porosimetry and compared with a porous NiO. The results obtained were:

- XRD revealed the presence of Co_3O_4 in the prepared cathode, and a loss of cobalt after its immersion.
- Raman studies confirmed at first the spinel structure of Co_3O_4 and a change of the Co_3O_4 structure into lithium–cobalt–nickel oxide ($LiCo_{1-y}Ni_yO_2$).
- XPS results show that the surface layer prepared is formed by $Ni(OH)_2$/NiO and Co_3O_4. After exposure the presence of Ni^{3+} was detected by XPS for the porous nickel and Co_3O_4-coated porous. This is probably due to the lithiation process NiO and NiO–Co, respectively.
- SEM micrographs revealed that the coated porous Ni suffered morphologic changes during the exposure and different morphologic in comparison with porous Ni. This could be explained by the formation of a lithium cobalt nickel oxide ($LiCo_{1-y}Ni_yO_2$) on the surface of nickel porous.
- Chemical analysis confirmed the dissolution of cobalt but an important reduction in the solubility of nickel in the prepared cathode.
- The cobalt oxide on porous nickel sample presented after its immersion similar porosity and higher pore size than the porous nickel.

These results showed that the cathode prepared by electrodeposition technique presented a good properties to be used as an alternative cathode for MCFC. Further research on the characterization in single cell will be performed.

Acknowledgment

This work was carried out in the frame of a Spain–France Exchange Agreement, CSIC/CNRS (Ref. 2002FR0007, no. 11433).

References

[1] S.T. Kuk, Y.S. Song, S. Suh, J.Y. Kim, K. Kim, J. Mater. Chem. 11 (2001) 630–635.
[2] T. Fukui, S. Ohara, H. Okawa, T. Hotta, M. Naito, J. Power Sources 86 (2000) 340–346.
[3] F. Li, H.Y. Chen, C.M. Wang, K.A. Hu, J. Electroanal. Chem. 531 (2002) 53–60.
[4] P. Ganesan, H. Colon, B. Haran, B.N. Popov, J. Power Sources 115 (2003) 12–18.
[5] H. Okawa, J.H. Lee, T. Hotta, S. Ohara, S. Takahashi, T. Shibahashi, Y. Yamamasu, J. Power Sources 131 (2004) 251–255.
[6] L. Daza, C.M. Rangel, J. Baranda, M.T. Casais, M.J. Martínez, J.A. Alonso, J. Power Sources 86 (2000) 329–333.
[7] J. Soler, T. González, M.J. Escudero, T. Rodrigo, L. Daza, J. Power Sources 106 (2002) 189–195.
[8] M.J. Escudero, X.R. Nóvoa, T. Rodrigo, L. Daza, J. Power Sources 106 (2002) 196–205.
[9] S.G. Kim, S.P. Yoon, J. Han, S.W. Nam, T.H. Lim, S.A. Hong, H.C. Lim, J. Power Sources 112 (2002) 109–115.
[10] F.J. Pérez, D. Duday, M.P. Hierro, C. Gómez, M. Romero, M.T. Casais, J.A. Alonso, M.J. Martínez, L. Daza, J. Power Sources 72 (2000) 309–315.
[11] L. Mendoza, V. Albin, M. Cassir, A. Galtayries, J. Electroanal. Chem. 548 (2003) 95–107.
[12] M.J. Escudero, T. Rodrigo, L. Mendoza, M. Cassir, L. Daza, J. Power Sources 140 (2005) 81–87.
[13] A. Durairajan, H. Colon-Mercado, B. Haran, R. White, B. Popov, J. Power Sources 104 (2002) 157–168.
[14] P. Ganesan, H. Colon, B. Haran, R. White, B.N. Popov, J. Power Sources 111 (2002) 109–120.
[15] C. Belhomme, M. Cassir, J. Devynck, G. Gregoire, J. Mater. Sci. 35 (2000) 2683–2688.
[16] E. Antolini, J. Mater. Sci. 35 (2000) 1501–1505.
[17] S.T. Kuk, Y.S. Song, K. Kim, J. Power Sources 83 (1999) 50–56.
[18] V.G. Hadjiev, M.N. Iliev, I.V. Vergilov, J. Phys. C: Solid State Phys. 21 (1988) L199–L201.
[19] H. Shirai, Y. Moriopka, I. Nakagawa, J. Phys. Soc. Jpn. 51 (1982) 592–597.
[20] J.E. Herrera, D.E. Resasco, J. Phys. Chem. B 107 (2003) 3738–3746.
[21] W. Huang, R. Frec, Solid State Ionics 86–88 (1996) 395–400.
[22] S.G. Kang, S.Y. Kang, K.S. Ryu, S.H. Chang, Solid State Ionics 120 (1999) 155–161.
[23] M. Inaba, Y. Todzuka, H. Yoshida, Y. Grincourt, A. Tasaka, Y. Tomiuda, Z. Ogumi, Chem. Lett. (1995) 889–990.

[24] B.H. Ryu, S.P. Yoon, J. Han, S.W. Nam, T.H. Lim, S.A. Hong, K.B. Kim, Electrochim. Acta 50 (2004) 189–198.
[25] N.S. McIntyre, M.G. Cook, Anal. Chem. 47 (1975) 2208–2213.
[26] D.B. Mitton, J. Walton, G.E. Thompson, Surf. Interf. Anal. 20 (1993) 36–42, 267–275.
[27] I.G. Casella, M.R. Guascito, J. Electroanal. Chem. 476 (1999) 54–63.